Inorganic Chemistry

Article

pubs.acs.org/IC

Metal–Metal Interactions in C_3-Symmetric Diiron Imido Complexes Linked by Phosphinoamide Ligands

Subramaniam Kuppuswamy,[†] Tamara M. Powers,[‡] Bruce M. Johnson,[§] Mark W. Bezpalko,[†] Carl K. Brozek,[‖] Bruce M. Foxman,[†] Louise A. Berben,[§] and Christine M. Thomas*[,†]

[†]Department of Chemistry, Brandeis University, 415 South Street MS 015, Waltham, Massachusetts 02454, United States

[‡]Department of Chemistry and Chemical Biology, Harvard University, Cambridge, Massachusetts 02139, United States

[§]Department of Chemistry, University of California—Davis, Davis, California 95616, United States

[‖]Department of Chemistry, Massachusetts Institute of Technology, 77 Massachusetts Avenue, Cambridge, Massachusetts 02139-4307, United States

S *Supporting Information*

ABSTRACT: The tris(phosphinoamide)-bridged Fe^{II}Fe^{II} diiron complex Fe(μ-^{i}PrNPPh$_2$)$_3$Fe(η^2-^{i}PrNPPh$_2$) (**1**) can be reduced in the absence or presence of PMe$_3$ to generate the mixed-valence Fe^{II}Fe^{I} complexes Fe(μ-^{i}PrNPPh$_2$)$_3$Fe(PPh$_2$NH^{i}Pr) (**2**) or Fe(μ-^{i}PrNPPh$_2$)$_3$Fe(PMe$_3$) (**3**), respectively. Following a typical oxidative group transfer procedure, treatment of **2** or **3** with organic azides generates the mixed-valent Fe^{II}Fe^{III} imido complexes Fe(^{i}PrNPPh$_2$)$_3$Fe≡NR (R = ^{t}Bu (**4**), Ad (**5**), 2,4,6-trimethylphenyl (**6**)). These complexes represent the first examples of first-row bimetallic complexes featuring both metal–ligand multiple bonds and metal–metal bonds. The reduced complexes **2** and **3** and imido complexes **4**–**6** have been characterized via X-ray crystallography, Mössbauer spectroscopy, cyclic voltammetry, and SQUID magnetometry, and a theoretical description of the bonding within these diiron complexes has been obtained using computational methods. The effect of the metal–metal interaction on the electronic structure and bonding in diiron imido complexes **4**–**6** is discussed in the context of similar monometallic iron imido complexes.

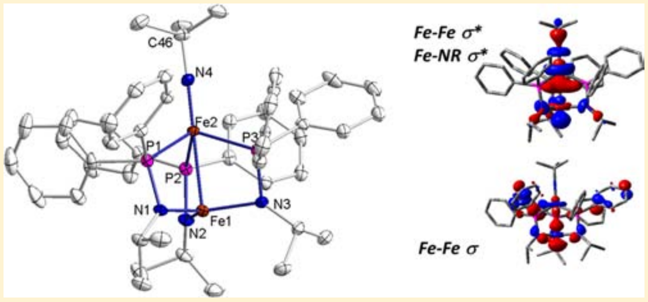

INTRODUCTION

Use of multiple metal centers to affect multielectron transfer chemistry is a strategy utilized in biological processes, and chemists have recently sought to harness this enhanced redox activity using rationally designed multimetallic clusters.[1−6] Among these examples, a new paradigm has emerged in which the three-center/four-electron bonding in bimetallic complexes with axial ligands is thought to lead to the "superelectrophilic" reactivity displayed by putative dirhodium carbene and nitrene catalytic intermediates during C–H activation/functionalization processes (Chart 1, **A**).[7] To further examine this phenomenon, Berry and co-workers have been targetting complexes that feature both metal–metal and metal–ligand multiple bonds.[8−10] The first complex of this type to be reported was the nitrido species [Ru(dPhf)$_4$Ru≡N] (Chart 1, **B**, dPhf = *N*,*N*′-diphenylformamidinate), and although this complex was too reactive to be isolated, EXAFS and resonance Raman spectroscopy revealed an unusually long Ru–N bond distance (1.76 Å) and an unusually low ν(Ru≡N) stretch (847.2 cm^{-1}) as compared to analogous monometallic Ru nitrides.[10] The weakened Ru–nitrido linkage, which is rationalized by delocalization over the two Ru centers, manifests itself in enhanced reactivity toward aryl C–H amination.[8] Similarly, a W–W oxo complex (Chart 1, **C**) has shown enhanced reactivity toward O-atom transfer compared to monometallic oxos, although in this case the W–O distance appears to be similar to those in mononuclear compounds.[9] Notably, these two examples represent the only reports of

Chart 1. Examples of Complexes Reported in the Literature Featuring Both Metal–Metal and Metal–Ligand Multiple Bonds[a]

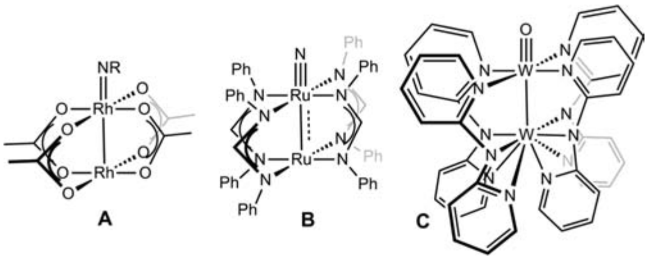

[a]Proposed dirhodium nitrene intermediates formed during catalytic C–H activation/functionalization (**A**), diruthenium nitride complex (**B**), and ditungsten oxo complex (**C**).

Received: September 28, 2012
Published: December 24, 2012

bimetallic complexes featuring both metal–metal bonds and metal–ligand multiple bonds, and no examples featuring first-row metals have been reported to date.

In contrast to their second- and third-row counterparts,[11] far less is understood about the electronic structure and reactivity of bimetallic complexes composed of high-spin first-row metals. Several non-organometallic dinuclear Fe complexes have been synthesized and feature both high-spin states and strong metal–metal interactions.[12–14] For example, the C_3-symmetric complex $Fe_2(DPhF)_3$ (DPhF = diphenylformamidate) has a very short Fe–Fe distance (2.2318(8) Å) and an $S = 7/2$ ground state. Examination of the electronic structure reveals that arranging the electrons in a high-spin configuration in a metal–metal σ, π, and δ bonding/antibonding manifold still results in an Fe–Fe bond order of 1.5 (a computed value of 1.15 was determined using multiconfigurational wave function analysis).[14–16] In light of this, we were curious to ascertain whether metal–ligand multiple bonding would also be feasible in a high-spin bimetallic regime.

Our group has been utilizing ambidentate phosphinoamide ligands to construct early/late heterobimetallic platforms,[17] but we recently discovered that such ligands can also support combinations of late transition metals.[18,19] For example, the $S = 4$ diiron complex $Fe(\mu\text{-}^iPrNPPh_2)_3Fe(\eta^2\text{-}^iPrNPPh_2)$ (**1**) features a zwitterionic combination of two iron(II) centers in close proximity.[19] Herein we turn our attention to the multielectron redox processes and reactivity of **1**, including group transfer to form a diiron imido functionality trans to an iron–iron bond.

■ RESULTS

Synthesis of 2–6. Reduction of **1** with excess Na/Hg amalgam proceeded smoothly, as predicted by cyclic voltammetry (CV),[19] to generate the one-electron-reduced complex $Fe(\mu\text{-}^iPrNPPh_2)_3Fe(PPh_2NH^iPr)$ (**2**, Scheme 1). Rather than an η^2-bound phosphinoamide ligand, the tris(phosphine)-ligated Fe center is now capped by a neutral phosphinoamine ligand. The presence of a proton on the phosphinoamine N atom was confirmed by an ν(N–H) stretch in the IR spectrum of **2** at 3383 cm^{-1}. To probe the source of this phosphinoamine proton, reduction of **1** was carried out in THF-d_8: The 3383 cm^{-1} stretch was still present in the resulting product, implying that the amine proton originated from decomposition of one of the phosphinoamide ligands rather than abstraction from solvent. The ^{1}H NMR resonances of **2** are broad and paramagnetically shifted, but identification of nine tentatively assigned resonances confirms two inequivalent phosphinoamide/amine ligand environments.

Scheme 1

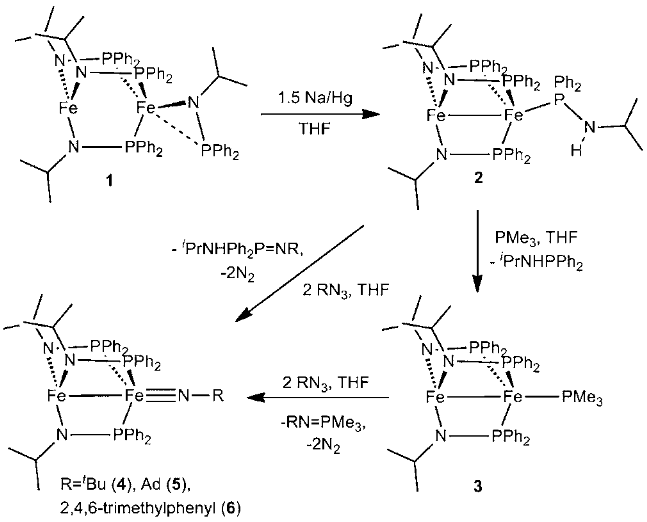

The neutral phosphinoamine in **2** can be easily substituted via treatment with excess PMe_3 to generate $Fe(^iPrNPPh_2)_3Fe(PMe_3)$ (**3**). In this case, the ^{1}H NMR spectrum has only five discernible resonances which can be assigned to the PMe_3 and phosphinoamide ligands. Addition of two equivalents of organic azide, RN_3 (R = ^{t}Bu, Ad, Mes (2,4,6-trimethylphenyl)), to either **2** or **3** produces the imido complexes $Fe(^iPrNPPh_2)_3Fe{\equiv}NR$ (R = ^{t}Bu (**4**), Ad (**5**), Mes (**6**)) with concomitant formation of one equivalent of the corresponding phosphoranimine $^iPrNHPh_2P{=}NR$ or $RN{=}PMe_3$, respectively. Again, the ^{1}H NMR resonances of **4**–**6** are broad, but a symmetric environment is clearly indicated by the number of observed resonances (five for **4** and seven for **5** and **6**, see Experimental Section for tentative peak assignments).

X-ray Crystallography. The formulations of complexes **2**–**6** were confirmed via single-crystal X-ray diffraction. Complexes **2** and **3** are quite similar and reveal a pseudo-C_3-symmetric core geometry in which the tris(amido)Fe is trigonal pyramidal while the tris(phosphine)-ligated Fe center adopts a pseudotetrahedral geometry with an additional interaction to the second Fe center trans to the apical phosphine donor (Figure 1, Table 1). The Fe–Fe distances (2.4694(4) (**2**) and 2.4545(5) Å (**3**)) in these reduced complexes are significantly shorter than the Fe–Fe distance observed in the $Fe^{II}Fe^{II}$ starting material **1** (2.8684(6) Å).[19] This phenomenon can likely be attributed to both steric and electronic factors. Indeed, alleviation of the steric pressure imparted by the pseudobidentate apical phosphinoamide ligand in **1** (avg. P–Fe–P angle = 102.1°) may play a role in the expansion of the P–Fe–P angles in complexes **2** and **3** (avg. P–Fe–P angles = 106.8° and 106.7°, respectively), allowing the two Fe centers to approach each other. Additionally, reduction of the diiron core might be expected to populate Fe–Fe bonding orbitals, allowing for stronger metal–metal interactions in the reduced complexes.

Notably, the Fe–Fe distance in the related Fe^{II}–Fe^{II} complex $Fe(MesNP^iPr_2)_3FeCl$ is also fairly short 2.5855(4) Å.[19] Although the different substituents on the ligand donors complicate this comparison, the Fe–Fe distances in **2** and **3** are significantly shorter than the Fe–Fe distance in $Fe(MesNP^iPr_2)_3FeCl$, implying that the steric properties of the axial ligand are not solely responsible for the contraction of the Fe–Fe distance. From an electronic standpoint, there are two plausible explanations for the shortened metal–metal distance: (1) an increase in the metal–metal bond order as the result of populating an additional metal–metal bonding orbital upon reduction, or (2) an increase in the electron density of the reduced Fe center, providing increased covalency. On the basis of the concurrent contraction of the Fe–P distances upon reduction (from 2.49 Å in **1**[19] to 2.34 Å in **3**) and theoretically derived electronic structure arguments (vide infra), we favor the latter explanation. We note that while the Fe–P distances contract significantly upon reduction, there is no change in the Fe–N distances upon reduction from **1** to **2**/**3**, leading us to conclude that the reduction is centered at the tris(phosphine) Fe center. The lone example of a high-spin $Fe^{II}Fe^{I}$ trigonal lantern complex has a much shorter Fe–Fe distance (2.2318(8)

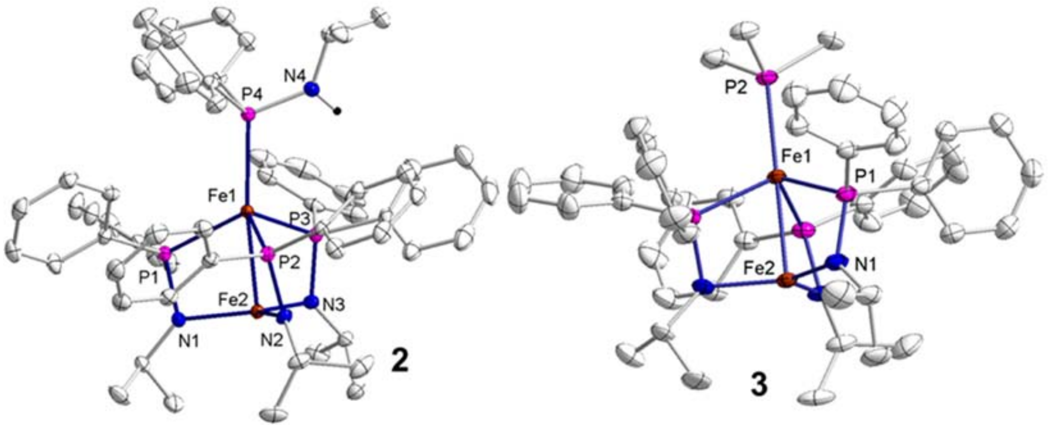

Figure 1. Displacement ellipsoid (50%) representation of **2** and **3**. Hydrogen atoms, except for the N-bound phosphinoamine proton, have been omitted for clarity.

Table 1. Relevant Interatomic Distances (Angstroms) and Angles (degrees) in Complexes 2−6

	2	3	4	5	6
Fe−Fe	2.4694(4)	2.4645(5)	2.5444(3)	2.5443(3)	2.5605(5)
Fe−P_{PN}	2.3658(6)	2.3453(4)	2.2378(5)	2.2166(4)	2.2694(7)
Fe−P_{PN}	2.3850(5)	2.3453(4)	2.2214(5)	2.2297(5)	2.2533(7)
Fe−P_{PN}	2.3594(6)	2.3453(4)	2.2287(4)	2.2371(4)	2.2550(7)
Fe−P_{PR3}	2.3701(6)	2.3538(7)			
Fe−N_{PN}	1.9697(16)	1.9663(13)	1.9457(12)	1.9548(12)	1.9558(19)
Fe−N_{PN}	1.9646(16)	1.9663(13)	1.9455(13)	1.9393(13)	1.944(2)
Fe−N_{PN}	1.9611(17)	1.9663(13)	1.9403(13)	1.9527(13)	1.949(2)
Fe−N_{NR}			1.6402(12)	1.6463(13)	1.670(2)
Fe−Fe−P_{PR3}	172.81(2)	180			
Fe−Fe−N_{NR}			179.45(4)	178.47(4)	177.99(7)
Fe−N−C_{NR}			178.23(12)	178.02(11)	177.72(18)
P_{PN}−Fe−P_{PN}	103.45(2)	106.706(13)	104.26(2)	105.682(16)	101.47(3)
P_{PN}−Fe−P_{PN}	108.71(2)	106.706(13)	104.92(2)	104.940(16)	102.83(3)
P_{PN}−Fe−P_{PN}	108.41(2)	106.706(13)	103.83(2)	101.965(17)	107.09(3)
N_{PN}−Fe−N_{PN}	119.23(7)	119.996(5)	121.44(5)	122.87(6)	114.15(8)
N_{PN}−Fe−N_{PN}	118.15(7)	119.996(5)	119.72(5)	122.00(5)	120.79(9)
N_{PN}−Fe−N_{PN}	122.56(7)	119.996(5)	118.84(5)	115.13(5)	125.06(9)

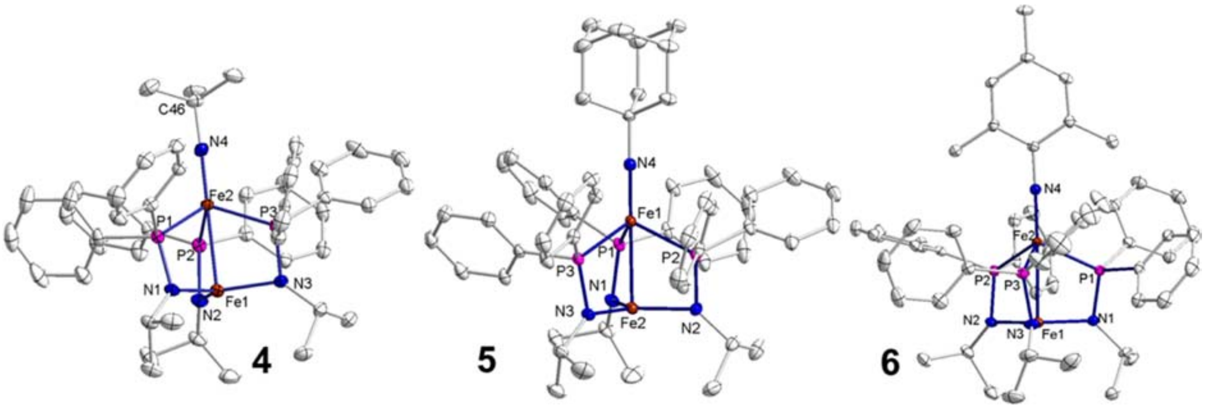

Figure 2. Displacement ellipsoid (50%) representation of **4**, **5**, and **6**. Hydrogen atoms have been omitted for clarity.

Å) than **3**,[15,20] likely a result of the differing orbital energies of the two Fe centers in **3** leading to weaker π and δ overlap.

The structures of imido complexes **4**−**6** were found to be rather similar to each other (Figure 2, Table 1). The distances from the phosphine-ligated Fe centers in **4**−**6** to the imido nitrogen atoms (Fe2−N4 = 1.6402(12) (**4**), 1.6463(13) (**5**), 1.670(2) Å (**6**)) are consistent with other C_3-symmetric Fe−imido complexes reported in the literature.[21−25] The local geometry of the two Fe centers in **4**−**6** is similar to that in **2** and **3** with contracted Fe2−P distances (avg = 2.23 (**4**, **5**) and 2.26 Å (**6**)) in line with previously reported low-spin tris(phosphine) Fe(III) imido complexes.[22,24,25] Thus, it appears as if **4**−**6** can reasonably be assigned as Fe(II)Fe(III)≡NR imido complexes with the imido-bound

Fe center in a low-spin state. The slightly elongated Fe−P distances in **6** compared to **4** and **5** can be attributed to the steric constraints associated with the mesityl imido substituent. In addition, the Fe−Fe distances are elongated to 2.5444(3), 2.5443(3), and 2.5605(5) Å in **4**, **5**, and **6**, respectively, as a result of strong σ and π donation from the imido fragment into Fe (effectively a trans influence), similar to the phenomenon observed in the Ru−Ru≡N complex reported by Berry and co-workers.[10] Notably, little effect on the distance between Fe and the imido nitrogen is observed as a consequence of the trans influence of the Fe−Fe bond, in contrast to the diruthenium system, suggesting relatively weak Fe−Fe bonding.

Mössbauer Spectroscopy. To better understand the electronic structure of the imido complex **4**, the ^{57}Fe Mössbauer spectrum was collected at 90 K (Figure 3). The Mössbauer spectrum of **4** is characterized by a single quadrupole doublet centered at $\delta = -0.06$ mm/s with a small quadrupole splitting ($|\Delta E_Q| = 0.54$ mm/s). This observation might initially suggest a fully delocalized mixed-valent $Fe^{2.5}Fe^{2.5}$ oxidation state assignment; however, the similarity of the Fe−N_{amide} bond distances between **3** and **4** and the aforementioned contraction of the Fe−P distances upon imido formation continue to suggest a more localized Fe(II)Fe(III) oxidation state assignment. The most striking aspect of this discrepancy is that even if the diiron system was undergoing rapid electron transfer, the two Fe centers remain in vastly different coordination environments and would, at the very least, be expected to lead to Mössbauer signals with different quadrupole splittings. Thus, two feasible possibilities that would explain the appearance of a single Mossbauer signal are (1) the accidental degeneracy of two Mössbauer signals or (2) a decreased signal for one of the Fe centers as a result of different excited state lifetimes (if the lifetime of one of the Fe centers is on the order of the Mössbauer experiment, it may be too broad to observe).[26,27]

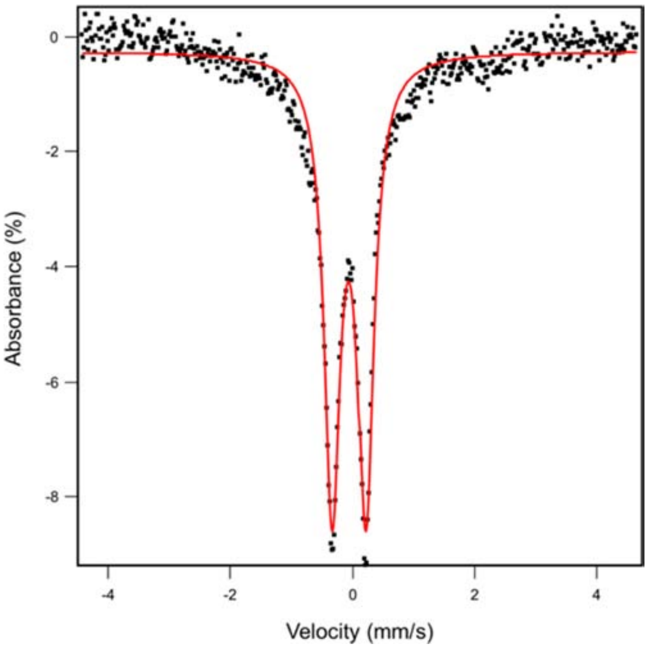

Figure 3. Zero-field ^{57}Fe Mössbauer spectrum of a solid sample of **4** at 90 K (black). Spectrum was fit (red) as a single-quadrupole doublet with $\delta = -0.06$ mm/s, $|\Delta E_Q| = 0.54$ mm/s.

To better understand this unusual Mössbauer result, computational methods were used to predict the isomer shift and quadrupole splitting for imido complex **4**. Indeed, two distinctly different Mössbauer parameters are predicted for the two Fe centers: $\delta = -0.23$ mm/s and $|\Delta E_Q| = 0.57$ mm/s for the imido-bound Fe center and $\delta = 0.16$ mm/s and $|\Delta E_Q| = 2.50$ mm/s for the tris(amido) Fe center. Thus, the appearance of just one signal does not appear to be the result of accidental overlap, and the quadrupole doublet observed appears to correspond to the imido Fe(III) ion. Although monomeric C_3-symmetric low-spin Fe(III) imido complexes have been reported,[21−25] the only example that has been characterized by Mössbauer spectroscopy is the tris(carbene)borate iron(III) imido complex, $PhB(MesIm)_3Fe{\equiv}NAd$, reported by Smith and co-workers.[28] The isomer shift of this compound is in good agreement with the signal observed for **4** ($\delta = -0.11$ mm/s). Mössbauer spectra of C_2-symmetric low-spin Fe(III) imido complexes have similarly low isomer shifts (e.g., (PDI)FeNR (PDI = pyridinediimine, R = alkyl), $\delta = -0.2$ to 0.04 mm/s),[29] while intermediate- to high-spin Fe(III) imido species tend to exhibit higher isomer shifts (e.g., (dipyrromethene)Fe(Cl)NAr, $\delta = 0.29$ mm/s).[30] At this time, we hypothesize that the signal for the trigonal Fe(II) center is unobservable as a result of differences in excited state lifetimes between the two Fe centers;[26,27] however, further studies (variable temperature, variable field) will be necessary to investigate this unusual phenomenon.

Magnetic Behavior. Solid state magnetic susceptibility measurements determined using SQUID magnetometry for **3** support the assignment of the trigonal Fe(II) center as high spin with four unpaired electrons, in combination with the pseudotetrahedral Fe(I) center which can only exist in one spin state with three unpaired electrons. At 300 K the observed magnetic moment is 7.97 μ_B, and this could be consistent with two different electronic models for the complex (Figure 4). If the two iron centers are considered to be ferromagnetically interacting, the predicted magnetic moment can be calculated from the $S = 7/2$ spin state by simple addition of the spins at each iron center. Accordingly, with $g = 2.0$, the predicted magnetic moment is 7.94 μ_B, which is in very good agreement with the measured value of 7.97 μ_B. However, it is known that tetrahedral Fe(I) complexes can possess g values higher than 2.0. For example, a combined synthetic and EPR study reported a pseudotetrahedral Fe(I) complex in which $g_1 = 2.61$, $g_2 = 2.0$, and $g_3 = 2.0$ were obtained.[24] This possibility means that the

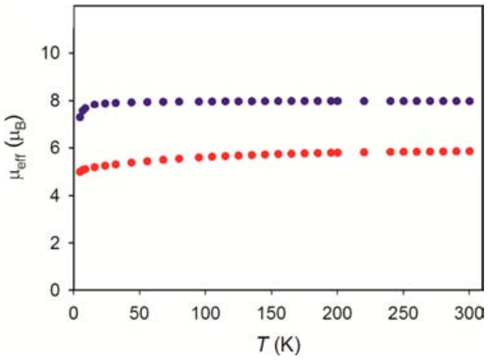

Figure 4. Magnetic susceptibility data for compounds **3** (blue) and **4** (red) in the solid state in an applied field of 0.1 T determined using SQUID magnetometry.

measured magnetic moment of 7.97 μ_B could feasibly correspond to the case where the iron centers are magnetically noninteracting. In a scenario with noninteracting iron centers, the calculated magnetic moment for **3** is 6.71 μ_B when g is assumed to be 2.0. If a value of $g = 2.35$ is assumed, this results in a calculated magnetic moment of 7.88 μ_B. Future work will probe the value of g in this system to yield a better understanding of the magnetic interactions observed. Our preliminary hypothesis, based on DFT calculations (vide infra), is that the iron centers are involved in a ferromagnetic exchange interaction. The very slight drop in the measured magnetic moment to 7.28 μ_B at 5 K is minor and could be attributed to several possibilities, such as intermolecular antiferromagnetic interactions or zero-field splitting. A solution magnetic moment for **3** was also determined using the Evans's method (7.66 μ_B at room temperature), and this value is in fairly good agreement with the solid state measurements.

The observed magnetic moment at 300 K for **4** is 5.85 μ_B, and this is consistent with an electronic structure that has five unpaired electrons (Figure 4). A similar analysis to that discussed above is also useful in this case. The pseudo-tetrahedral Fe(III)−imido center is best modeled as low spin with one unpaired electron, while the trigonal planar Fe(II) center is best described as high spin with four unpaired electrons. Once again, a situation in which these two iron centers are ferromagnetically coupled, with a calculated magnetic moment of 5.92 μ_B, would provide the best agreement of the electronic model with the measured magnetic susceptibility data, when $g = 2.00$. As for **3**, the measured magnetic moment of **4** falls only very slightly at 5 K, in this case to 4.98 μ_B. Once again this behavior suggests the presence of very weak intermolecular antiferromagnetic coupling or possibly a zero-field splitting effect. A solution magnetic moment for **3** was also determined using the Evans's method. At room temperature $\mu_{eff} = 5.52$ μ_B, and this value is in fairly good agreement with the solid state measurements.

Computational Investigation. Further insight into the electronic structure and Fe−Fe interactions in **3** and **4** was provided by the results of a computational investigation using density functional theory (DFT) and natural bond orbital (NBO) methods (BP86 functional, mixed basis set, see Supporting Information). Both the NBO charges and the Mulliken spin densities of the two Fe atoms in **3** suggest an Fe(II)Fe(I) configuration, with an $S = 3/2$ tris(phosphine)Fe center and an $S = 2$ tris(amido)Fe center (Table 2). Likewise, the Mulliken charges and spin densities calculated for complex **4** are consistent with an $S = 2$ tris(amido)Fe^{II} fragment linked to an $S = 1/2$ tris(phosphine)Fe^{III} center. As seen in the calculated frontier molecular orbital (MO) diagram of **3** (Figure 5), the Fe−Fe σ and σ^* orbitals are polarized as a result of the disparate coordination environments of the two Fe centers and, while the remainder of the MOs have some degree of orbital mixing, differing symmetries and mismatched orbitals energies lead to relatively poor π and δ overlap. NBO calculations reveal that the Fe−Fe bond (Figure 7), indeed, has unequal contributions from the two metals, with 65.4% of the orbital contribution coming from the tris(phosphine)Fe center and 34.6% from the tris(amido)Fe center.

Table 2. Computed Mulliken Spin Densities and Natural Charges (NBO) on the Two Fe Atoms in 3 and 4

	Fe_N		Fe_P	
	spin	charge	spin	charge
3	3.75	−0.83	2.77	−0.94
4	3.83	−0.56	0.75	0.83

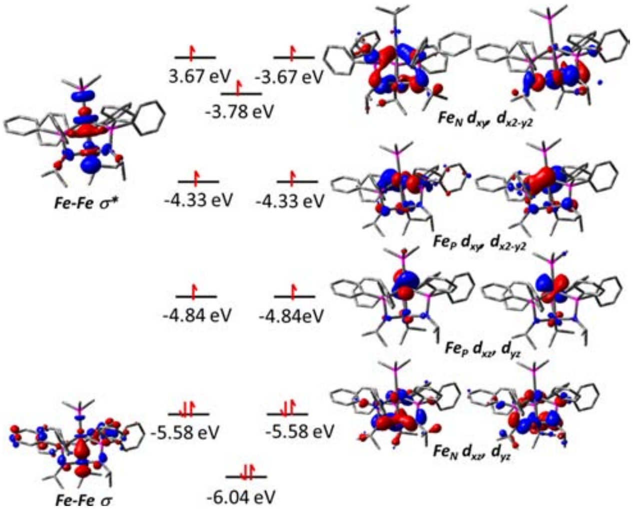

Figure 5. Pictorial representations of the calculated frontier molecular orbitals of **3** with primary orbital contributions and metal−metal bonds labeled.

The calculated MO diagram of imido complex **4** (Figure 6) is relatively similar, with the exception of the increased energies of the two LUMOs, which represent the Fe−imido π^* orbitals localized on a single Fe center. Qualitatively, the MO picture for the tris(phosphine)Fe center is similar to that of Peters' recently reported tris(phosphine)borane Fe imido complex;[25,31] however, the significant difference lies in the Fe−NR σ^* orbital. In this case, this orbital is also σ^* with respect to metal−metal bonding and much like complex **3** the Fe−Fe NBO is polarized, with 41.5% of the orbital contribution originating from the tris(amido)Fe and 58.5% from the tris(phosphine)Fe center (Figure 7).

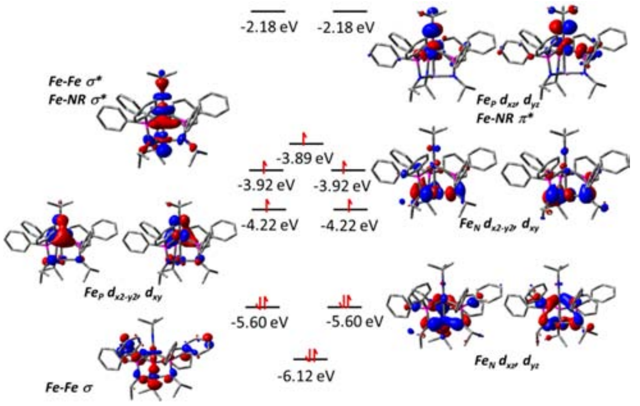

Figure 6. Pictorial representations of the calculated frontier molecular orbitals of **4** with primary orbital contributions and metal−metal bonds labeled.

Redox Behavior. To assess the effect of the metal−metal interactions on the redox behavior of the diiron imido complexes **4**−**6**, these complexes were probed using cyclic voltammetry (Figure 8). The cyclic voltammograms (CVs) of complexes **4** and **5** were nearly identical and showed both reversible oxidation and reduction events (see Supporting

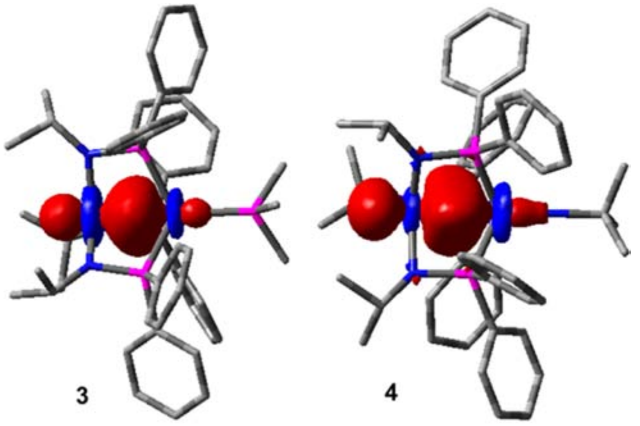

Figure 7. Calculated Fe−Fe natural bond orbitals (NBO) of **3** and **4**.

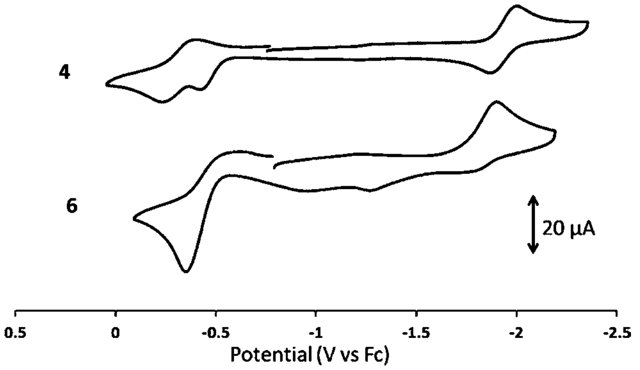

Figure 8. Cyclic volammograms of complexes **4** and **6** (2 mM in 0.4 M [^{n}Bu$_4$N][PF$_6$] in THF, scan rate = 100 mV/s).

Information for the CV of complex **5**). The $E_{1/2}$ of the reductive events for both **4** and **5** are −1.94 V vs ferrocene/ferrocenium, while the reversible second oxidative events are centered at $E_{1/2}$ = −0.32 and −0.35 V, respectively.[32] In contrast, oxidation of the monometallic tris(phosphine) Fe−imide PhB(CH$_2$PPh$_2$)$_3$Fe≡NAd is irreversible and centered at more positive potentials (−0.13 V) and the reversible reduction of this complex also occurs at more positive potential (−1.32 V).[22] Thus, the diiron imido complexes appear to be more electron rich than the monometallic tris(phosphino)borate analogues, allowing the homobimetallics to be oxidized more easily but discouraging reduction.

Unlike the alkyl-substituted imido complexes **4** and **5**, the aryl imido complex **6** only undergoes irreversible redox processes, as illustrated by an irreversible oxidation at −0.35 V and an irreversible reduction at −1.89 V in its CV (Figure 8). Here, the redox potentials of **6** are quite similar to those of **4** and **5**, but there are clear differences in the chemical stability of the resulting oxidized and reduced products. For comparison, the CV of the monometallic tris(phosphine) aryl imido complex PhB(CH$_2$PPh$_2$)$_3$Fe≡N(*p*-tolyl) was reported to feature an irreversible oxidation at −0.30 V and a reversible reduction at −1.35 V.[24]

DISCUSSION

While imido complexes **4**−**6**, at first glance, bear close resemblance to the tris(phosphino)borane[25] and tris(phosphino)borate[22,24] monoiron imido complexes of Peters and co-workers, replacement of boron with an additional Fe center adds another degree of complexity to the present system. Much like the tris(phosphino)borate complexes, **4**−**6** are zwitterions, with the tethered anion in this case being a tris(amido)Fe^{II} fragment rather than a tetrasubstituted borate anion (Chart 2). The most obvious difference between these two systems is the availability of orbitals on the tethered anion to participate in bonding to the imido−Fe unit. While a well-defined Fe−Fe interaction, albeit relatively weak, is present in complexes **4**−**6**, the borate anion in the tris(phosphino)borate systems simply plays the role of a noninteracting tethered anion. This results in both steric and electronic differences between the diiron complexes presented herein and the previously reported PhB(CH$_2$PPh$_2$)$_3$Fe≡NR complexes. The absence of an interaction with the apical boron allows the latter complexes to a adopt a geometry with contracted P−Fe−P angles near 90° with the Fe atom ~1.3 Å above the plane of the three phosphorus donors.[22,24] In the case of **4**−**6**, the Fe−Fe interaction leads to wider P−Fe−P angles as the Fe center approaches the plane of the phosphine donors (~0.9 Å).

These geometric differences lead to a less sterically protected imido fragment in the case of PhB(CH$_2$PPh$_2$)$_3$Fe≡NR and a much larger ligand field splitting as the antibonding d_{xz} and d_{yz} orbitals are raised in energy by stronger metal−phosphine ligand interactions (calculated Δ = 3.81 eV).[22] Close

Chart 2

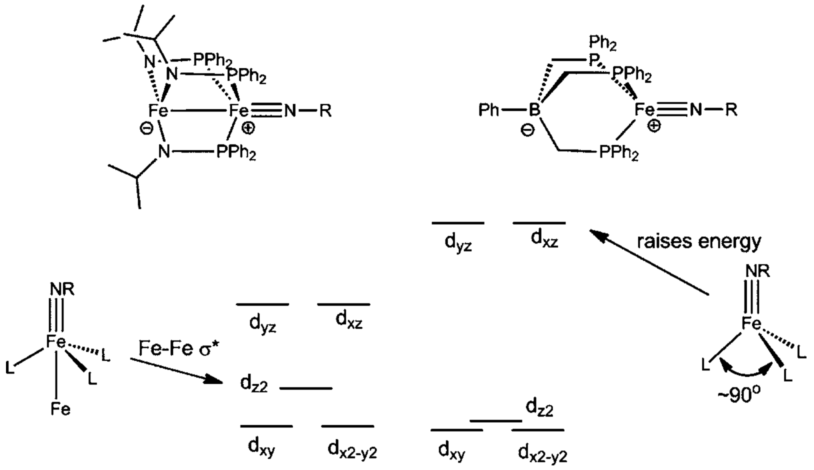

Table 3. X-ray Diffraction Data Collection and Refinement Details for **2**−**6**

	2	**3**	**4**	**5**	**6**
chemical formula	$C_{60}H_{69}Fe_2N_4P_4$	$C_{48}H_{60}Fe_2N_3P_4$	$C_{49}H_{60}Fe_2N_4P_3$	$C_{55}H_{66}Fe_2N_4P_3$	$C_{54}H_{62}Fe_2N_4P_3$
fw	1081.82	914.61	909.66	987.77	971.73
T (K)	120 K	120 K	120 K	120 K	120 K
λ (Å)	0.71073 Å	0.71073 Å	0.71073	0.71073	0.71073
a (Å)	13.2161(4)	16.1581(8)	19.098(2)	11.4641(6)	15.5760(9)
b (Å)	14.6236(4)	16.1581(8)	21.111(3)	20.2130(10)	18.7595(9)
c (Å)	28.4166(7)	23.4646(13)	11.5956(15)	21.6833(11)	17.0026(9)
α (deg)	90	90	90	90	90
β (deg)	95.398(1)	90	90	92.914(2)	91.353(3)
γ (deg)	90	120	90	90	90
V (Å^3)	5467.6(3)	5305.5(5)	4675.0(10)	5018.0(4)	4966.7(5)
space group	$P2_1/c$	P-3c1	$Pna2_1$	$P2_1/n$	$P2_1/n$
Z	4	4	4	4	4
D_{calcd} (g/cm^3)	1.314	1.145	1.292	1.307	1.299
μ (mm^{-1})	0.690	0.690	0.761	0.714	0.721
$R1$, $wR2^a$ ($I > 2\sigma$)	0.0323, 0.0932	0.0279, 0.0783	0.0235, 0.0564	0.0326, 0.0801	0.0453, 0.0898

$^a R1 = \Sigma(||F_o| - |F_c||)/\Sigma|F_o|$, $wR2 = \{\Sigma[w(F_o{}^2 - F_c{}^2)^2/\Sigma[w(F_o)^2]\}^{1/2}$.

examination of the frontier molecular orbital diagram of complex **4** shown in Figure 6 reveals a smaller ligand field splitting for the molecular orbitals most closely associated with the imido-bound Fe center (calculated Δ = 2.04 eV). Moreover, the d_{z2} orbital in the tris(phosphino)borate Fe imido systems is typically similar in energy to the d_{x2-y2} and d_{xy} orbitals,[22,31] but in the case of **4**, d_{z2} is raised in energy significantly as a result of the σ* interaction of this orbital with the appended Fe center.[33] The latter phenomenon may provide an explanation for the more negative reduction potentials observed for imido complexes **4**−**6**.

The tris(phosphino)borane-supported imido complex contains an Fe^{II} center but can nonetheless be included in the discussion. While the P−Fe−P angles in this system are similar to those in **4**−**6**, the Fe^{II} tris(phosphino)borane imido complex reported by Peters has a negligible Fe−B interaction, leading to a similar electronic structure to $PhB(CH_2PPh_2)_3Fe{\equiv}NR$.[25]

Interestingly, complexes **4**−**6** do not participate in group transfer reactions with CO or RNC even at elevated temperatures, in stark contrast to $PhB(CH_2PPh_2)Fe{\equiv}N$($p$-tolyl) which reacts readily with these substrates at room temperature.[24] This difference in reactivity may be attributed to a combination of steric effects (diminished accessibility of the imido fragment in complex **4** to incoming substrates) and electronic factors (better stabilization of the Fe−N π-symmetry orbitals of complex **4**).

The highest occupied molecular orbital in complexes **4**−**6** is a singly occupied orbital with both Fe−Fe σ* and Fe−N σ* character, implying that the reactivity patterns accessible with this class of iron imido complexes may be quite different. Due to the high-spin S = 5/2 nature of **4**−**6**, the Fe−Fe≡NR interaction is best described as a 3-center-3-electron bond with an Fe−Fe σ-bond order of 0.5. Small π contributions to the Fe−Fe bond order may exist, but there is little delocalization of electron density throughout the Fe−Fe≡NR π manifold as a result of mismatched atomic orbital energies between the two Fe centers with different coordination environments. The diminished reactivity of this diiron system with respect to its monometallic Fe−imido congeners is in stark contrast to the paradigm established for second- and third-row metal−ligand multiple bonded complexes that also feature metal−metal bonds. However, this difference can likely be attributed to the absence of extensive delocalization throughout the Fe−Fe≡NR chain.

■ CONCLUSIONS

In summary, we synthesized a series of unusual bimetallic diiron imido complexes featuring both metal−metal bonding and metal−ligand multiple bonding. These compounds are synthetically accessible using the well-precedented method of oxidative group transfer from an organic azide to an Fe^I center. While the $Fe^{II}Fe^{III}$ imido complexes do not appear to display any promising group transfer reactivity, future work will focus on the readily accessible multielectron redox behavior of these species and the reactivity of resulting reduced and oxidized derivatives.

■ EXPERIMENTAL SECTION

General Considerations. Unless specified otherwise, all manipulations were performed under an inert atmosphere using standard Schlenk or glovebox techniques. Glassware was oven dried before use. Benzene, pentane, diethyl ether, tetrahydrofuran, and toluene were dried using a Glass Contours solvent purification system. All solvents were stored over 3 Å molecular sieves prior to use. Benzene-d_6 (Cambridge Isotopes) was degassed via repeated freeze−pump−thaw cycles and dried over 3 Å molecular sieves. Ph_2PNH^iPr,[34,35] Ph_2PNK^iPr,[19] and $[Fe(^iPrNPPh_2)_3Fe(^iPrNPPh_2)]$ (**1**)[19] were synthesized using literature procedures. Anhydrous $FeCl_2$ was purchased from Strem Chemicals and used after 12 h drying at 100 °C under vacuum. NMR spectra were recorded at ambient temperature on a Varian Inova 400 MHz instrument. Chemical shifts are reported in δ (ppm). For ^1H and $^{13}C\{^1H\}$ NMR spectra, the solvent resonance was used as an internal reference and for $^{31}P\{^1H\}$ NMR spectra 85% H_3PO_4 was referenced as an external standard (0 ppm). IR spectra were recorded on a Varian 640-IR spectrometer controlled by Resolutions Pro software. UV−vis spectra were recorded on a Cary 50 UV−vis spectrophotometer using Cary WinUV software. Elemental analyses were performed at Complete Analysis Laboratory Inc., Parsippany, NJ. Solution magnetic moments were measured using Evans' method.[36,37]

Electrochemistry. CV measurements were carried out in a glovebox under a dinitrogen atmosphere in a one-compartment cell using a CH Instruments electrochemical analyzer. A glassy carbon electrode and platinum wire were used as the working and auxiliary electrodes, respectively. The reference electrode was $Ag/AgNO_3$ in THF. Solutions of electrolyte (0.40 M $[^nBu_4N][PF_6]$ in THF) and analyte (2 mM) were also prepared in the glovebox. All potentials are reported versus an internal ferrocene/ferrocenium reference.

Mössbauer Spectroscopy. Iron-57 Mössbauer spectra were measured on a constant acceleration spectrometer (SEE Co, Minneapolis, MN) with a Janis SVT-100 cryostat. Isomer shifts are quoted relative to α-Fe foil (<25 μm thick) at room temperature. The Fe foil standard spectrum has line widths Γ (fwhm) of 0.292 and 0.326 mm/s for the doublets within the ±4 mm/s window when measured outside the cryostat at room temperature. Samples of **4** were prepared using approximately 30 mg of sample suspended in paratone-N oil. Data were analyzed using a package written by E. R. King and modified by E. V. Eames in Igor Pro (Wavemetrics) using a simple model consisting of Lorentzian line shapes with optional asymmetry.

X-ray Crystallography Procedures. All operations were performed on a Bruker-Nonius Kappa Apex2 diffractometer using graphite-monochromated Mo Kα radiation. All diffractometer manipulations, including data collection, integration, scaling, and absorption corrections, were carried out using the Bruker Apex2 software.[38] Preliminary cell constants were obtained from three sets of 12 frames. Data collection and refinement details are presented in Table 3, and fully labeled diagrams and data collection and refinement details are included in the Supporting Information file.

Magnetic Susceptibility Measurements. Magnetic measurements were recorded using a Quantum Designs MPMS XL magnetometer at 0.1 T. The sample was contained under nitrogen in a gel cap and suspended in the magnetometer in a plastic straw. The magnetic susceptibility was adjusted for diamagnetic contributions using Pascal's constants.

Computational Details. All calculations except those for predicting Mössbauer parameters were performed using Gaussian09-E.01[39] for the Linux operating system. Density functional theory calculations were carried out using a combination of Becke's 1988 gradient-corrected exchange functional[40] and Perdew's 1986 electron correlation functional[41] (BP86). For open-shell systems, unrestricted wave functions were used in energy calculations. A mixed basis set was employed using the LANL2TZ(f) triple-ζ basis set with effective core potentials for iron,[42−44] Gaussian09's internal 6-311+G(d) for atoms bonded directly to the metal centers (nitrogen and phosphorus), and Gaussian09's internal LANL2DZ basis set (equivalent to D95 V[45]) for carbon and hydrogen. Starting with crystallographically determined geometries as a starting point, when available, the geometries were optimized to a minimum, followed by analytical frequency calculations to confirm that no imaginary frequencies were present. NBO analysis was performed using NBO 3.1,[46] as implemented by Gaussian09.

The ORCA 2.9.1[47] computational package was used to optimize the geometry and simulate Mössbauer parameters of a model of compound **4**. We employed the pure-DFT functional BP86[38,39] and the Alrichs TZV basis sets[48] and polarization functions for all calculations. The SCF equations were converged tightly to 10^{-8} Hartree in the total energy, and the open-shell systems were treated with spin-unrestricted Kohn−Sham determinants. The Broken Symmetry feature was used to specify one unpaired electron on the imido-bound iron site, while four unpaired electrons were imposed on the second site.

We constructed the model compound by starting from the crystal structure and simplifying all −R to methyl groups. The entire structure was optimized with a tolerance of 5×10^{-6} Hartree for each energy change. The EPR/NMR module was used to simulate the Mössbauer parameters. Both the spin−spin and spin−orbit operators were evaluated using the coupled-perturbed method to solve the spin−orbit component. This calculation provided values of η, the asymmetry parameter, and ρ, the s-orbital electron density at the absorbing nucleus. The quadrupolar splittings of both iron nuclei were calculated from the values of η. To correlate the computed ρ to an isomer shift value, we calculated ρ for a series of compounds with known isomer shifts and, using their linear relationship, determined isomer shifts from a best-fit line. The known compounds were simple iron salts covering a range of oxidation states and treated in a manner identical to **4** by starting from reported crystal structures.

Synthesis of Fe(^{i}PrNPPh$_2$)$_3$Fe(^{i}PrNHPPh$_2$) (2). A 0.5% Na/Hg amalgam was prepared from 0.059 g of Na (2.6 mmol) and 11.8 g of Hg.[49] To this vigorously stirred amalgam in 30 mL of THF was added a solution of **1** (1.84 g, 1.7 mmol) in THF (30 mL). The resulting purple mixture gradually turned brown during the course of the reaction. After 4 h, the resulting brown solution was filtered away from the amalgam. Volatiles were removed under vacuum, and the remaining crude brown material was washed with cold pentane (3 × 10 mL). Subsequent extraction with toluene followed by solvent removal yielded an analytically pure brown crystalline solid of **2** (1.49 g, 81%). ^{1}H NMR (400 MHz, C_6D_6): δ 27.6 (iPr-Me, μ-ligand), 14.9 (iPr-Me, terminal ligand), 11.5 (iPr-CH, terminal ligand), 3.6 (Ph, terminal ligand), 3.4 (Ph, terminal ligand), 2.0 (*p*-Ph, μ-ligand), 1.0 (*m*-Ph, μ-ligand), −9.1 (Ph, terminal ligand), −10.5 (*o*-Ph, μ-ligand) (isopropyl methine proton on the bridging ligand and amine proton on the terminal ligand were not observed).[50] IR (KBr solution cell, benzene): 3383 cm^{-1}. UV−vis (C_6H_6) λ_{max}, nm (ε, L mol^{-1} cm^{-1}): 304 (16 000), 366 (7500), 506 (2200). Evans' method (C_6D_6): 7.40 μ_B. Anal. Calcd for $C_{60}H_{69}Fe_2N_4P_4$: C, 66.62; H, 6.43; N, 5.18. Found: C, 66.49; H, 6.37; N, 5.17.

Synthesis of Fe(^{i}PrNPPh$_2$)$_3$Fe(PMe$_3$) (3). A solution of **2** (0.53 g, 0.49 mmol) in THF (15 mL) was chilled to −32 °C, and to this solution, PMe$_3$ (0.10 mL, 0.98 mmol) was added dropwise over 5 min. The resulting mixture was then warmed to room temperature and stirred for 12 h to form **3**. Volatiles were removed under vacuum. The byproduct (free ligand) was removed by washing with pentane to obtain **3** as an analytically pure greenish-brown crystalline solid (0.38 g, 85%). ^{1}H NMR (400 MHz, C_6D_6): δ 76.6 (PMe$_3$), 28.9 (iPr-Me), 3.3 (*p*-Ph), 1.0 (*m*-Ph), −12.7 (*o*-Ph) (isopropyl methine proton was not observed).[50] UV−vis (C_6H_6) λ_{max}, nm (ε, L mol^{-1} cm^{-1}): 301 (26 000), 366 (11 000), 502 (2800). Evans' method (C_6D_6): 7.66 μ_B. Anal. Calcd for $C_{48}H_{60}Fe_2N_3P_4$: C, 63.04; H, 6.61; N, 4.59. Found: C, 63.17; H, 6.64; N, 4.67.

Synthesis of Fe(^{i}PrNPPh$_2$)$_3$Fe≡N^{t}Bu (4). A solution of **2** (0.50 g, 0.46 mmol) in THF (10 mL) was chilled to −32 °C, and to this ^{t}BuN$_3$ (0.092 g, 0.92 mmol) was added dropwise over a period of 5 min. The reaction mixture immediately turned purple, and the resulting mixture was continuously stirred for an additional 2 h to ensure completion of the reaction. Volatiles were removed under vacuum, and the crude materials were washed with pentane to remove soluble impurities and ^{i}PrNHPh$_2$P═N^{t}Bu. Extraction of the remaining purple material in toluene followed by solvent removal under vacuum yielded analytically pure **4** (0.34 g, 81%). ^{1}H NMR (400 MHz, C_6D_6): δ 14.9 (iPr-Me), 10.8 (N-tBu), 7.4 (Ph), 5.3 (Ph), 0.9 (Ph) (isopropyl methane proton is not observed).[50] UV−vis (C_6H_6) λ_{max}, nm (ε, L mol^{-1} cm^{-1}): 326 (16 000), 532 (3700). Evans' method (C_6D_6): 5.52 μ_B. Anal. Calcd for $C_{49}H_{60}Fe_2N_4P_3$: C, 64.70; H, 6.65; N, 6.16. Found: C, 64.80; H, 6.57; N, 6.18.

Synthesis of Fe(^{i}PrNPPh$_2$)$_3$Fe≡NAd (5). A solution of **2** (0.43 g, 0.39 mmol) in THF (10 mL) was chilled to −32 °C, and to this a THF solution of AdN$_3$ (0.14 g, 0.75 mmol) was added dropwise over the period of 10 min. The reaction mixture immediately turned purple and was continuously stirred for an additional 2 h to ensure completion of the reaction. Volatiles were removed under vacuum, and the crude materials were washed with pentane to remove the soluble impurities and ^{i}PrNHPh$_2$P═NAd. Extraction of the remaining purple material in toluene followed by solvent removal under vacuum yielded analytically pure **5** (0.35 g, 91%). ^{1}H NMR (400 MHz, C_6D_6): δ 15.0 (iPr-Me), 9.5 (Ad), 7.9 (Ph), 5.3 (Ph), 0.9 (Ph), 0.5 (Ad), −0.2 (Ad) (isopropyl methane resonance is not observed).[50] UV−vis (C_6H_6) λ_{max}, nm (ε, L mol^{-1} cm^{-1}): 326 (14 000), 530 (3300). Evans' method (C_6D_6): 5.25 μ_B. Anal. Calcd for $C_{55}H_{66}Fe_2N_4P_3$: C, 66.88; H, 6.73; N, 5.67. Found: C, 66.93; H, 6.69; N, 5.61.

Synthesis of Fe(^{i}PrNPPh$_2$)$_3$Fe≡NMes (6). A solution of **3** (0.30 g, 0.33 mmol) in THF (6 mL) was chilled to −32 °C, and to this 2,4,6-trimethylphenylazide (0.11 g, 0.66 mmol) was added dropwise over a period of 5 min. The reaction mixture gradually turned purple, and the resulting mixture was continuously stirred for an additional 12 h to ensure completion of the reaction. Volatiles were removed under vacuum, and the crude materials were washed with pentane to remove soluble impurities and $Me_3P{=}NMes$. Extraction of the remaining purple material in toluene followed by solvent removal under vacuum yielded analytically pure **6** (0.23 g, 72%). ^1H NMR (400 MHz, C_6D_6): δ 14.4 (iPr-CH_3), 8.0 (Ph), 6.1 (Ph), 1.0 (Ph), −5.9 (N-Mes), −22.5 (N-Mes), −35.9 (N-Mes) (isopropyl methane proton is not observed).[50] UV−vis (C_6H_6) λ_{max}, nm (ε, L mol^{-1} cm^{-1}): 328 (21700), 540 (5700), 680 (1900). Evans' method (C_6D_6): 5.80 μ_B. Anal. Calcd for $C_{54}H_{62}Fe_2N_4P_3$: C, 66.75; H, 6.43; N, 5.77. Found: C, 66.78; H, 6.47; N, 5.73.

■ ASSOCIATED CONTENT

Ⓢ Supporting Information

Additional spectroscopic data, computational details, and crystallographic data in CIF format. This material is available free of charge via the Internet at http://pubs.acs.org.

■ AUTHOR INFORMATION

Corresponding Author

*E-mail: thomasc@brandeis.edu.

Author Contributions

The manuscript was written through contributions of all authors. All authors have given approval to the final version of the manuscript.

Notes

The authors declare no competing financial interest.

■ ACKNOWLEDGMENTS

This material is based upon work supported by Brandeis University and the Department of Energy under Award No. DE-SC0004019. C.M.T. is grateful for a 2011 Sloan Research Fellowship. The authors also thank Dr. Theodore A. Betley for insightful discussions and assistance with Mössbauer spectroscopy.

■ REFERENCES

(1) Kanady, J. S.; Tsui, E. Y.; Day, M. W.; Agapie, T. *Science* **2011**, *333*, 733−736.

(2) Tsui, E. Y.; Kanady, J. S.; Day, M. W.; Agapie, T. *Chem. Commun.* **2011**, *47*, 4189−4191.

(3) Fout, A. R.; Zhao, Q.; Xiao, D. J.; Betley, T. A. *J. Am. Chem. Soc.* **2011**, *133*, 16750−16753.

(4) Harris, T. D.; Zhao, Q.; Sanchez, R. H.; Betley, T. A. *Chem. Commun.* **2011**, *47*, 6344−6346.

(5) Powers, T. M.; Fout, A. R.; Zheng, S.-L.; Betley, T. A. *J. Am. Chem. Soc.* **2011**, *133*, 3336−3338.

(6) Zhao, Q.; Betley, T. A. *Angew. Chem., Int. Ed.* **2011**, *50*, 709−712.

(7) Berry, J. F. *Dalton Trans.* **2012**, *41*, 700−713.

(8) Long, A. K. M.; Timmer, G. H.; Pap, J. S.; Snyder, J. L.; Yu, R. P.; Berry, J. F. *J. Am. Chem. Soc.* **2011**, *133*, 13138−13150.

(9) Nippe, M.; Goodman, S. M.; Fry, C. G.; Berry, J. F. *J. Am. Chem. Soc.* **2011**, *133*, 2856−2859.

(10) Pap, J. S.; DeBeer George, S.; Berry, J. F. *Angew. Chem., Int. Ed.* **2008**, *47*, 10102−10105.

(11) Cotton, F. A.; Murillo, C. A.; Walton, R. A. *Multiple Bonds Between Metal Atoms*; Springer Science and Business Media, Inc.: New York, 2005.

(12) Timmer, G. H.; Berry, J. F. *C. R. Chim.* **2012**, *15*, 192−201.

(13) Cotton, F. A.; Daniels, L. M.; Matonic, J. H.; Murillo, C. A. *Inorg. Chim. Acta* **1997**, *256*, 277−282.

(14) Cotton, F. A.; Feng, X.; Murillo, C. A. *Inorg. Chim. Acta* **1997**, *256*, 303−308.

(15) Zall, C. M.; Zherebetskyy, D.; Dzubak, A. L.; Bill, E.; Gagliardi, L.; Lu, C. C. *Inorg. Chem.* **2012**, *51*, 728−736.

(16) Cotton, F. A.; Daniels, L. M.; Falvello, L. R.; Matonic, J. H.; Murillo, C. A. *Inorg. Chim. Acta* **1997**, *256*, 269−275.

(17) Thomas, C. M. *Comments Inorg. Chem.* **2011**, *32*, 14−38.

(18) Kuppuswamy, S.; Cooper, B. G.; Bezpalko, M. W.; Foxman, B. M.; Powers, T. M.; Thomas, C. M. *Inorg. Chem.* **2012**, *51*, 1866−1873.

(19) Kuppuswamy, S.; Bezpalko, M. W.; Powers, T. M.; Turnbull, M. M.; Foxman, B. M.; Thomas, C. M. *Inorg. Chem.* **2012**, *51*, 8225−8240.

(20) Cotton, F. A.; Daniels, L. M.; Murillo, C. A. *Inorg. Chim. Acta* **1994**, *224*, 5−9.

(21) Thomas, C. M.; Mankad, N. P.; Peters, J. C. *J. Am. Chem. Soc.* **2006**, *128*, 4956−4957.

(22) Brown, S. D.; Peters, J. C. *J. Am. Chem. Soc.* **2005**, *127*, 1913−1923.

(23) Nieto, I.; Ding, F.; Bontchev, R. P.; Wang, H.; Smith, J. M. *J. Am. Chem. Soc.* **2008**, *130*, 2716−2717.

(24) Brown, S. D.; Betley, T. A.; Peters, J. C. *J. Am. Chem. Soc.* **2003**, *125*, 322−323.

(25) Moret, M.-E.; Peters, J. C. *Angew. Chem., Int. Ed.* **2011**, *50*, 2063−2067.

(26) Gütlich, P.; Bill, E.; Trautwein, A. X. *Mössbauer Spectroscopy and Transition Metal Chemistry*; Springer Science and Business Media, Inc.: New York, 2001.

(27) Bancroft, G. M. *Mössbauer Spectroscopy: An Introduction for Inorganic Chemists and Geochemists*; McGraw-Hill: New York, 1973.

(28) Scepaniak, J. J.; Harris, T. D.; Vogel, C. S.; Sutter, J.; Meyer, K.; Smith, J. M. *J. Am. Chem. Soc.* **2011**, *133*, 3824−3827.

(29) Bowman, A. C.; Milsmann, C.; Bill, E.; Turner, Z. R.; Lobkovsky, E.; DeBeer, S.; Wieghardt, K.; Chirik, P. J. *J. Am. Chem. Soc.* **2011**, *133*, 17353−17369.

(30) King, E. R.; Hennessy, E. T.; Betley, T. A. *J. Am. Chem. Soc.* **2011**, *133*, 4917−4923.

(31) Tangen, E.; Conradie, J.; Ghosh, A. *J. Chem. Theory Comput.* **2007**, *3*, 448−457.

(32) The first irreversible oxidative feature appears to be an artifact of events occurring at negative potentials and diminishes in intensity when potentials less than −0.8 V are not accessed (see Supporting Information).

(33) An alternative explanation for the higher relative energy of the d_{z^2} orbital might be the increased linearity of the Fe-imido linkage (Fe−N−C angle) as a result of the added steric constraints in this system.

(34) Sisler, H.; Smith, N. *J. Org. Chem.* **1961**, *26*, 611−613.

(35) Poetschke, N.; Nieger, M.; Khan, M. A.; Niecke, E.; Ashby, M. T. *Inorg. Chem.* **1997**, *36*, 4087−4093.

(36) Sur, S. K. *J. Magn. Reson.* **1989**, *82*, 169−173.

(37) Evans, D. F. *J. Chem. Soc.* **1959**, 2003−2005.

(38) *Apex 2: Version 2 User Manual, M86-E01078*; Bruker Analytical X-ray Systems: Madison, WI, 2006.

(39) Frisch, M. J.; Trucks, G. W.; Schlegel, H. B.; Scuseria, G. E.; Robb, M. A.; Cheeseman, J. R.; Scalmani, G.; Braone, V.; Mennucci, B.; Petersson, G. A. e. a. *Gaussian 09*, Revision A.1; Gaussian, Inc.: Wallingford, CT, 2009.

(40) Becke, A. D. *Phys. Rev. A* **1988**, *38*, 3098−3100.

(41) Perdew, J. P. *Phys. Rev. B* **1986**, *33*, 8822−8824.

(42) Hay, P. J.; Wadt, W. R. *J. Chem. Phys.* **1985**, *82*, 299−310.

(43) Roy, L. E.; Hay, P. J.; Martin, R. L. *J. Chem. Theory Comput.* **2008**, *4*, 1029−1031.

(44) Ehlers, A. W.; Bohme, M.; Dapprich, S.; Gobbi, A.; Hollwarth, A.; Jonas, V.; Kohler, K. F.; Stegmann, R.; Veldkamp, A.; Frenking, G. *Chem. Phys. Lett.* **1993**, *208*, 111−114.

(45) Dunning, T. H.; Hay, P. J. In *Modern Theoretical Chemistry*, Schaefer, H. F., Ed.; Plenum: New York, 1976; Vol. 3, pp 1−28.

(46) Glendening, E. D.; Reed, A. E.; Carpenter, J. E. *NBO Version 3.1*.

(47) Neese, F. *ORCA−an ab initio, Density Functional and Semiempirical program package*, Version 2.9.1; University of Bonn: Bonn, Germany, 2008.

(48) Schäfer, A.; Horn, H.; Ahlrichs, R. *J. Chem. Phys.* **1992**, *97*, 2571.

(49) The authors recognize that Na/Hg is not the safest or most environmentally friendly option when it comes to reductants; however, it was chosen in this case since it operates at a mild potential (−2.2 V vs Fc) to avoid over-reduction (the CV of complex **1** has a quasi-

reversible reduction at −1.98 V, but an irreversible event also occurs at −2.64 V).

(50) Tentative assignments of resonances in the ^{1}H NMR spectra were based on relative peak integrations, relative peaks widths, and comparison between similar species.